Spectral link of the generalized Townsend-Perry constants in turbulent boundary layers

Björn Birnir,[1] Luiza Angheluta,[2] John Kaminsky,[1] and Xi Chen[3]

[1]*Center for Complex and Nonlinear Science and Department of Mathematics, University of California, Santa Barbara, Santa Barbara, California 93106, USA*

[2]*The Njord Centre, Department of Physics, University of Oslo, P.O. Box 1048, 0316 Oslo, Norway*

[3]*Institute of Fluid Mechanics, Beihang University, Beijing, China*

(Received 3 July 2020; accepted 25 August 2021; published 21 October 2021)

We propose a first minimal theory for boundary layer turbulence that captures very well the profile of the mean-square velocity fluctuations in the streamwise direction and give a quantitative prediction of the Townsend-Perry constants. Our theory is based on connecting all moments of velocity fluctuations as a function of the distance to the wall with the turbulent energy spectrum. A similar spectral theory was proposed in G. Gioia and P. Chakraborty [Phys. Rev. Lett. **96**, 044502 (2006)] to explain the friction factor and the von Kármán law in G. Gioia, N. Guttenberg, N. Goldenfeld, and P. Chakraborty [Phys. Rev. Lett. **105**, 184501 (2010)]. We generalized it by including fluctuations in the wall-shear stress and the streamwise velocity. The theoretical predictions for the mean velocity and mean-square fluctuations reproduce the shape of the velocity profiles in the buffer and inertial layer obtained from wind tunnel experiments.

DOI: 10.1103/PhysRevResearch.3.043054

I. INTRODUCTION

Turbulence is a ubiquitous phenomenon encountered in very diverse natural systems, from the large-scale atmosphere [1] and oceans [2] all the way down to quantum fluids [3], as well as in engineered systems, such as pipelines, heat exchangers, wind turbines, etc. It relates to the complex fluid dynamics that orchestrate the interactions of flow eddies spanning many length scales and generating non-Gaussian statistics of velocity increments. The statistical properties of these turbulent fluctuations are fundamentally changed when the flow is confined by the presence of solid walls or boundaries [4,5]. In contrast to the bulk turbulence, which is statistically homogeneous and isotropic, the wall-bounded turbulence is characterized by statistically anisotropic properties. Namely, there is a net mean flow in the streamwise direction along the wall and different flow structures form depending on their distance to the wall. We typically differentiate between four flow regions as moving away from the wall [6,7]: (i) The *viscous region* is closest to the wall and dominated by viscous flows, (ii) the *buffer layer* makes the transition from viscous to turbulent flows and is where detached eddies initially form, (iii) the *inertial layer* where the turbulent eddies form from the attached eddies and the log laws of the wall applies, and (iv) the *wake*, the fully developed energetic region where turbulent fluctuations can be described by homogeneous turbulence.

A theory presenting the form of the averaged velocity and averaged velocity fluctuation squared, formulating the influence of both attached and detached eddies on these quantities, holds the possibility of explaining a wide variety of boundary flows, ranging from pipe flows to atmospheric flows and extending to the flows observed on other planets. In this paper, we formulate a step toward a more complete theory of phenomena observed in flows sheared by a boundary.

The log law of the wall refers to the logarithmic dependence of the mean flow velocity (MVP) with the distance to the wall, also known as the Prandtl and von Kármán law, and is one of the staples of wall-bounded turbulence. It reads as

$$U = \frac{1}{\kappa}\log(\tilde{y}) + B, \tag{1}$$

where κ is the *universal* von Kármán constant that is independent of the microscopic flow characteristics and relates to generic features such as space dimension and geometry. The distance to the wall y and the mean fluid velocity u along the wall are typically expressed in the "wall units" determined by the wall shear stress τ_0. This is because τ_0 is an important theoretical concept that is also experimentally measurable. The friction velocity $u_\tau = \sqrt{\langle\tau_0\rangle/\rho}$, which is set by the wall shear stress τ_0 and the kinematic viscosity ν and enters in the unit rescalings as $\tilde{U} = U/u_\tau$ and $\tilde{y} = yu_\tau/\nu$. The constant fluid density is ρ and the B is a dimensionless constant that is fitted to experimental data, e.g., Ref. [8].

Other log laws have been empirically found and argued for and relate to the logarithmic dependence of *any* moment of the streamwise flow velocity with the wall distance. Namely, the streamwise velocity fluctuations, $\tilde{u} = u/u_\tau$, $\tilde{u} = \tilde{U} + \tilde{w}$, also follow the log law of the wall in its second moment as

$$\langle\tilde{w}^2\rangle = -A_1\log(\tilde{y}) + B_1, \tag{2}$$

where the coefficients A_1 and B_1, also called the Townsend-Perry constants, were first measured by Perry and Chong [9,10]. It has been experimentally observed that the log law generalizes to any moment of the streamwise velocity fluctuations,

$$\langle \tilde{w}^{2p} \rangle^{1/p} = -A_p \log(\tilde{y}) + B_p, \tag{3}$$

which can also be shown assuming Gaussian fluctuations, even though the dependence of A_p and B_p on p turns out to be sub-Gaussian, as confirmed both experimentally and numerically [11]. The sub-Gaussian behavior was explained in Ref. [12] using the stochastic closure theory (SCT) of turbulence [13,14] and the analysis was improved in Ref. [15]. Both of these studies used the results from homogeneous turbulence [16] and made an assumption about the form of the fluctuating shear stress in the inertial layer based on physical principles.

By now, there is a consensus on the universality of these log laws in the inertial region for different wall-bounded turbulent flows and its importance for practical applications. However, we are still lacking a unified theoretical framework in which these asymptotic log laws can be derived systematically with minimal phenomenological input and in a way that connects the buffer and inertial regions. We propose such a first theory for the wall-bounded turbulence using the spectral link between the statistics of near-wall fluctuations and the turbulent kinetic energy that starts already in the buffer region. It turns out that what happens in the buffer region plays a key role in setting up eddies that then facilitate energy cascade and sufficient turbulence for the log laws to emerge in the inertial layer.

Previous studies have derived the asymptotic log laws in various ways. One way of deriving the log law for the MVP is to use the attached eddy hypothesis of Townsend [17], but the problem with the attached eddy hypothesis is that it has not been successfully formulated theoretically until now. We show that the spectral link provides us with a way of mathematically formulating the attached eddy hypothesis. This spectral link was already applied to the MVP in Ref. [18], and we are able to extend it to derive the profile of the mean of the second moment both in the buffer and in the inertial region. We provide a physical explanation of the $1/k$ spectrum that has been observed in the buffer region as being the shrinking and speeding up of vortex tubes whose cross-sections consist of detached eddies. The $1/k$ scaling turns out to be critical to understand the second and higher moments of the streamwise velocity fluctuations. It also allows us to improve the MVP profile from the spectral theory proposed in Ref. [18]. Our spectral theory provides quantitative predictions for all the Townsend-Perry constants and the generalized Townsend-Perry constants that enter in the log laws of the higher moments and are in agreement with the predictions from the SCT of turbulence [13,14].

In this paper, we propose a generalization of the spectral theory that includes fluctuations in the streamwise velocity due to an essentially fluctuating wall shear stress. These velocity fluctuations are characterized by an interplay between the Kolmogorov-Obukhov energy spectrum and the $1/k$ spectrum in the buffer and inertial layers. Figure 1 shows our spectral theory predictions of the profiles of the mean velocity and mean-square fluctuations across the viscous, buffer, and inertial layers.

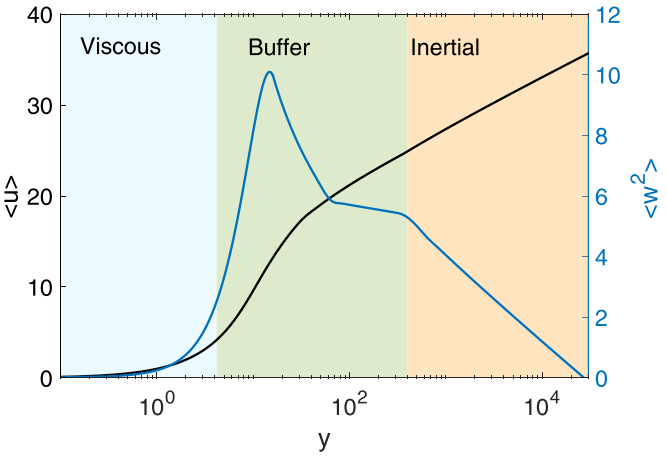

FIG. 1. Theoretical predictions from the spectral theory for the MVP $\langle u \rangle$ and mean-square velocity fluctuations $\langle w^2 \rangle$ (dimensionless variables in wall units).

Figure 1 illustrates a statistical theory of the mean velocity and its variation across the boundary layer. It starts with the Prandtl-von Kármán law in the inertial region but extends the mean velocity across the boundary and viscous layers by means of detached and attached eddies. The latter is a mathematical formulation of Townsend's theory [17] that connects all the eddies, and the former is similar. The theory produces the log law of the variation and its higher moments in the inertial region and permits an evaluation of the Townsend-Perry constants and their generalizations.

The rest of the paper is structured as follows. We introduce the spectral theory from Ref. [18] and generalize it for the second moment in Sec. II and higher moments in Sec. III. This produces the log law of the wall in Eq. (2) for the velocity fluctuations and its higher moments in Eq. (3). Then in Sec. IV, we derive the functional form of the mean-square fluctuations in the viscous layer and the inertial layer. In Sec. V, we use the attached eddy hypothesis and the SCT [13,14] to derive the form of the Townsend-Perry and the generalized Townsend-Perry constants. This allows us to derive the streamwise fluctuations in the wall shear stress and remove the assumption made in Refs. [12] and [15]. Using theory-informed data analysis, we can construct the Townsend-Perry constants and the generalized Townsend-Perry constants. In Sec. VI, we extend the formulas for the mean-square fluctuations to the buffer layer and the energetic wake. In Sec. VII, we compare the predicted MVP and mean-square velocity profile from this spectral theory to experimental data. In Sec. VIII, we conclude with a discussion on the proposed spectral theory and the role that Townsend's attached eddies play in it.

II. THE SPECTRAL THEORY

The typical velocity of an inertial eddy of size s can be obtained by integrating out the kinetic energy contained in all

eddies of sizes up to s as introduced in Ref. [18],

$$v_s^2 = \int_{1/s}^{\infty} E(k)dk, \tag{4}$$

where the kinetic energy spectrum follows the Kolmogorov-Obukhov scaling with cutoffs in the injection scale and viscous scales,

$$E(k) = c_d(\eta k)\frac{2}{3}(\kappa_\epsilon \epsilon)^{2/3}k^{-5/3}c_e(Rk), \tag{5}$$

with $\frac{2}{3}(\kappa_\epsilon\epsilon)^{2/3}k^{-5/3}$ being the Kolmogorov-Obukhov spectrum and $c_d(\eta k)$ and $c_e(Rk)$ the phenomenological dimensionless corrections functions in the dissipative (set by the Kolmogorov scale η) and energetic range (set by the system size R), respectively; κ_ϵ is a dimensionless parameter, ϵ is the turbulent energy dissipation rate, $\eta = \nu^{3/4}\epsilon^{-1/4}$ is the viscous length scale, and R is the largest length scale in the flow. The dissipative correction function is typically an exponential cutoff function $c_d(\eta k) = \exp(-\beta_d \eta k)$, and the energetic-range (wake) correction function is $c_e(Rk) = (1 + [\beta_e/(Rk)]^2)^{-17/4}$, which is the form that was proposed by von Kármán. β_d and β_e are nonnegative fitting constants that can be adjusted to data. By the change of variables $\xi = sk$, we recast Eq. (4) as

$$v_s^2 = (\kappa_\epsilon \epsilon s)^{2/3} I\Big(\frac{\eta}{s}, \frac{s}{R}\Big), \tag{6}$$

where the spectral function I is given by the formula

$$I\Big(\frac{\eta}{s}, \frac{s}{R}\Big) = \frac{2}{3}\int_1^{\infty} e^{-\xi\beta_d\eta/s}\xi^{-5/3}\left(1 + \left(\frac{\beta_e s}{R\xi}\right)^2\right)^{-17/6} d\xi. \tag{7}$$

The integral sums the energies of all eddies of a smaller radius than s and computes their contribution to the energy of the eddy of radius s. This is the energy (or spectral) formulation of the attached eddy hypothesis of Townsend [17]. The I function correctly captures the buffer layer as the transition from the viscous to the inertial layer and the asymptotic of the MVP in the energetic wake. The asymptotic values are such that in the inertial layer $I = 1$ and in the viscous layer $I = 0$. The I function combines the Kolmogorov-Obukhov theory with the observed spectrum in the viscous layer, the inertial layer, and the wake and is thus able to capture the transition from one layer to the next. In Ref. [18], it was used to give the details of the MVP. In this paper, we will use it to capture the profile of mean-square fluctuations.

In the buffer layer, a different scaling of the attached eddies comes into play; this is the k^{-1} scaling of the spectrum that has been debated in the literature, but clearly shows up in recent simulations and experiments in the middle of the buffer layer; see Fig. 9(a) in Ref. [19] and Fig. 12(b) in Ref. [20]. In the spectral theory, the corresponding I function for this scaling regime is

$$I_b\Big(\frac{\eta}{s}, \frac{s}{R}\Big) = \frac{2}{3}s^{-\frac{2}{3}}\int_1^{\infty} e^{-\xi\beta_d\frac{\eta}{s}}\xi^{-1}\left(1 + \left(\frac{\beta_e s}{R\xi}\right)^2\right)^{-\frac{17}{6}} d\xi, \tag{8}$$

where the subscript b stands for "buffer." The mean velocity is primarily influenced by the I function, whereas the variation (fluctuation squared) is greatly influenced by the I_b function in the buffer layer. I is associated with the Kolmogorov-Obukhov energy cascade $k^{-5/3}$ in the inertial layer, whereas I_b is associated with the k^{-1} scaling in the buffer layer. We will take I_b to be zero outside the buffer layer.

The splitting of the near-wall region based on different scaling of the spectrum was proposed by Perry and Chong [9] who used it to build an interpolation model for MVP and the variation; this model was improved in Ref. [21].

We find that in the boundary and buffer layers the isotropic $k^{-5/3}$ (K41) and 1/k scalings capture both the mean energy and the fluctuation squared dependence on the attached eddies quite well. In the inertial layer, intermittency becomes important and we need the full intermittency corrections (K62) to model the generalized Townsend-Perry constants; see below. This is consistent with the results in Ref. [22]. Namely, intermittency is important in the streamwise direction and becomes more pronounced toward the wall. However, it does not seem to play a role in the energy transfer of the attached and detached eddies away from the wall.

III. GENERALIZED LOG LAW

In this section, we will generalize the derivation of the MVP in Ref. [18] by adding a fluctuation to the streamwise mean velocity, $U(y)$, namely,

$$u = U + w. \tag{9}$$

In Ref. [18] the mean shear stress at the distance y from the wall that controls the momentum transfer across layers is given by $\langle\tau_t\rangle = \kappa_\tau \rho y v_y U'$, where the $U' = dU/dy$, v_y is the typical eddy velocity at distance y from the wall, ρ is the fluid density, and κ_τ is the dimensionless proportionality factor. When velocity fluctuations are included, the *instanteneous* shear stress becomes:

$$\tau_t = \kappa_\tau \rho y v_y (U' + w'). \tag{10}$$

The mean energy dissipation rate is related to the wall shear stress as $\langle\epsilon\rangle = \langle\tau_t\rangle U'/\rho$ [18], and including the fluctuations, this becomes

$$\epsilon = \tau_t(U' + w')/\rho. \tag{11}$$

The eddy velocity for an eddy with radius $s = y$ at the distance y from the wall is the same as in Ref. [18] and as discussed above,

$$v_y = (\kappa_\epsilon \epsilon y)^{1/3}\sqrt{I}, \tag{12}$$

where $I(\eta/y, R/y)$ is the integral from Eq. (7) and κ_ϵ is a dimensionless proportionality factor. In the inertial layer, $I = 1$ and $\kappa_\epsilon = 4/5$ according to Kolmogorov's 4/5 law.

Eliminating ϵ and v_y from the three equations above, we obtain that

$$\tau_t = (\kappa_\epsilon \kappa_\tau^3)^{1/2}\rho y^2 u'^2 I^{3/4}. \tag{13}$$

The viscous shear stress is $\rho\nu u'$ so the total shear stress, including the contribution from the fluctuation, is [17]

$$\tau_t + \rho\nu u' = \tau_0(1 - y/R). \tag{14}$$

Equation (14) is derived from the Navier-Stokes equation for channel flow; see Ref. [17], Chapter 5. The addition of the energy integral is due to Gioia *et al.* in Ref. [18]; it is the mathematical formulation of Townsend's attached eddy theory that connects all the eddies. Our assumption is that the wall shear stress τ_0 is also a quantity that fluctuates about its mean value.

The equations defining the stress in Ref. [17], Chapter 5 can be integrated from any point y_1 in the flow to give

$$\tau_t + \rho\nu u' = \tau_1 + \frac{\partial p_1}{\partial x}(y - y_1), \tag{15}$$

where p_1 is the pressure at the distance y_1 from the wall and τ_1 and $\frac{\partial p_1}{\partial x}$ are fluctuating quantities. This shows that the turbulence is driven not only by the boundary fluctuations but also by the (total) fluctuating stress at any point in the flow. It explains why the boundary can be cut away and the turbulence persists in numerical simulations [5,23]. It has been observed in experiment that the wall stress can become negative and then Eq. (15) must be used instead of Eq. (14).

We change the rescaled variables in the wall units written here in terms of the friction factor f: $\tilde{y} = yRe\sqrt{f}/R$, $\tilde{u} = u/(U\sqrt{f})$, and $\tilde{w} = w/(U\sqrt{f})$ and let $f = \langle\tau_0\rangle/\rho U^2$. The Reynolds number is $Re = \frac{UR}{\nu}$, where U is the mean velocity of the flow (for example, the flux divided by the cross-sectional area of a pipe) and R is the largest length scale in the flow (for example, the radius of a pipe). Then, the equation above becomes

$$\tilde{\kappa}^2\tilde{y}^2(\tilde{u}')^2 I^{3/4} + \tilde{u}' = \frac{\tau_0}{\langle\tau_0\rangle}\left(1 - \frac{\tilde{y}}{Re\sqrt{f}}\right). \tag{16}$$

We will present three derivations of U and w below based on Eq. (16). First we make an approximation in this section to connect with the the Prandtl-von Kármán log law for $\tilde{U}$ and the Townsend-Perry log law for $\langle\tilde{w}^2\rangle$ in the intertial range. Then in the next section, we derive the real formulas for U and w, showing that the log laws are the leading terms in the inertial range. These formulas also produce the Generalized Townsend-Perry constants. Finally, in Sec. VI, we integrate the differential equations for U and w; this is necessary because I is a function of y the distance from the wall and get the expressions for $\tilde{U}$ and $\langle\tilde{w}^2\rangle$ that can be compared with simulations and experimental data.

If we let $\tilde{y} \to 0$, $\tilde{w} \to 0$ and integrate, we get the law of the viscous layer

$$\tilde{U} = \tilde{y}, \tag{17}$$

the laminar profile being

$$\tilde{U} = \left(\tilde{y} - \frac{\tilde{y}^2}{2Re\sqrt{f}}\right). \tag{18}$$

In the large Reynolds number limit, solving just for the mean velocity, we obtain the Prandtl-von Kármán law

$$\tilde{U} = \frac{1}{\tilde{\kappa}}\log(\tilde{y}) + D. \tag{19}$$

If we solve for both the mean velocity and the fluctuation in the large Reynolds number limit, we get that

$$\tilde{U} + \tilde{w} = \frac{\sqrt{\tau_0}}{\langle\tau_0\rangle^{1/2}\tilde{\kappa}}\log(\tilde{y}) + C. \tag{20}$$

This is consistent with Eq. (19) in the sense that if $\tilde{w} = 0$, then $\sqrt{\tau_0} = \langle\tau_0\rangle^{1/2}$ and we recover Eq. (19). Thus squaring Eq. (20) and taking the average, we obtain the log law of the mean-square fluctuation gives that

$$\langle\tilde{w}^2\rangle = -A\log(\tilde{y}) + B, \tag{21}$$

where $A = -\frac{2C\langle\sqrt{\tau_0}\rangle - 2D\sqrt{\langle\tau_0\rangle}}{\tilde{\kappa}\sqrt{\langle\tau_0\rangle}}$ and $B = C^2 - D^2$ are the Townsend-Perry constants. The full formulas in the next section show that Eq. (21) is the leading term with $C = D$.

To simplify the notation, we will now drop the tildes from all the variables with the dimensionless units implicitly assumed, unless otherwise stated.

IV. TOWNSEND-PERRY LAW

We will now use Eq. (16) to find the general form of the average of the fluctuations squared as a function of the distance to the wall. Integrating Eq. (16) in the limit of $I = 0$ and subtracting U gives

$$\langle w^2\rangle = \frac{\langle\tau_0^2\rangle - \langle\tau_0\rangle^2}{\langle\tau_0\rangle^2}\left(y - \frac{y^2}{2Re\sqrt{f}}\right)^2. \tag{22}$$

In the inertial layer $I = 1$ and ignoring the small $O(1/y^4)$ term, we get that

$$U + w = \frac{1}{2\kappa^2 y} + 2\frac{\sqrt{\tau_0}}{\kappa\sqrt{\langle\tau_0\rangle}}\sqrt{1 - \frac{y}{2Re\sqrt{f}}} - 2\frac{\sqrt{\tau_0}}{\kappa\sqrt{\langle\tau_0\rangle}}\tanh^{-1}\left(\sqrt{1 - \frac{y}{2Re\sqrt{f}}}\right) + K, \tag{23}$$

by a symbolic computation, where K is an integration constant. The average velocity satisfies

$$U = \frac{1}{2\kappa^2 y} + \frac{2}{\kappa}\sqrt{1 - \frac{y}{2Re\sqrt{f}}} - \frac{2}{\kappa}\tanh^{-1}\left(\sqrt{1 - \frac{y}{2Re\sqrt{f}}}\right) + K', \tag{24}$$

where K' is another constant, because τ_0 becomes $\langle\tau_0\rangle$. Thus, the fluctuating velocity is given by

$$w = 2\frac{(\sqrt{\tau_0} - \sqrt{\langle\tau_0\rangle})}{\kappa\sqrt{\langle\tau_0\rangle}}\sqrt{1 - \frac{y}{2Re\sqrt{f}}} - 2\frac{(\sqrt{\tau_0} - \sqrt{\langle\tau_0\rangle})}{\kappa\sqrt{\langle\tau_0\rangle}}\tanh^{-1}\left(\sqrt{1 - \frac{y}{2Re\sqrt{f}}}\right) + C, \tag{25}$$

where $C = K - K'$. By taking the mean-square average and looking at the leading-order term for high Re number, we obtain

$$\langle w^2\rangle \sim 2C\frac{(\langle\sqrt{\tau_0}\rangle - \sqrt{\langle\tau_0\rangle})}{\kappa\sqrt{\langle\tau_0\rangle}}\log\left(\frac{y}{Re\sqrt{f}}\right) + h.o.t., \tag{26}$$

which reduces to Eq. (21). For higher-order moments $\langle w^{2p}\rangle^{1/p}$ the similar term, linear in $\tanh^{-1}(x)$ and multiplied by $2C$, is of leading order,

$$\langle w^{2p}\rangle^{1/p} \sim 2C\frac{\langle(\sqrt{\tau_0} - \sqrt{\langle\tau_0\rangle})^p\rangle^{1/p}}{\kappa\sqrt{\langle\tau_0\rangle}}\log\left(\frac{y}{Re\sqrt{f}}\right) + h.o.t. \tag{27}$$

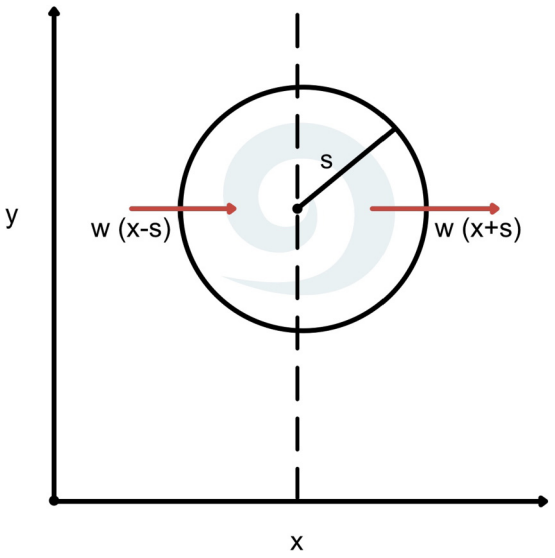

FIG. 2. The eddy of radius s and the variation in the fluctuations across it in the x (streamwise) direction.

These formulas establish the log dependence of the second moment of the fluctuations, with the Townsend-Perry constants, and the log dependence of the higher moments of the fluctuations, with the generalized Townsend-Perry constants, and justify formulas in Eq. (2) and Eq. (3). Together, Eq. (2) and Eq. (3) can be called the generalized log law of the wall.

V. DERIVATION OF THE GENERALIZED TOWNSEND-PERRY CONSTANTS

We consider the dependence of the fluctuation w on the distance x along the wall to understand the Townsend-Perry constants. So far we have only considered $w(y)$ as a function of the distance y from the wall, but $w(x, y)$ obviously depends on both variables x and y. If we consider the eddy depicted in Fig. 2, then we see that the difference in momentum in the x direction, across the eddy, is given by

$$\rho(w(x+s) - w(x-s)) \sim 2\rho s w_x, \tag{28}$$

for y fixed, where $w_x = \frac{d}{dx}w$.

This means that the total turbulent stress, across a vertical surface at x, denoted by a dotted line on Fig. 2 for an eddy of radius $s \sim y$, is

$$\tau_0 = \tau_t + \tau_x, \tag{29}$$

where $\tau_x = 2\kappa_\tau \rho y w_x v_y$, analogous to formula Eq. (10) above. Then we get, using Eq. (12) and

$$\epsilon = (\tau_t + \tau_x)(U' + w_x)\rho, \tag{30}$$

that

$$\tau_t + \tau_x = \kappa^2 \rho I^{3/4} y^2 (U' + w_x)^2, \tag{31}$$

where prime denotes the derivative with respect to y, and

$$\begin{aligned}(\tau_t + \tau_x)^{1/2} &= \kappa \rho^{1/2} I^{3/8} y (U' + w_x) \\ &= \langle \tau_0 \rangle^{1/2} + \kappa \rho^{1/2} I^{3/8} y |w_x|,\end{aligned} \tag{32}$$

since both parts must be positive. The derivation is completely analogous to the derivation in Sec. III, but here with w varying in the x direction and $w_y = 0$. This gives that for y fixed,

$$\begin{aligned}\tau_0^{1/2} - \langle \tau_0 \rangle^{1/2} &= (\tau_t + \tau_x)^{1/2} - \langle \tau_0 \rangle^{1/2} \\ &= \kappa \rho^{1/2} I^{3/8} y |w_x|.\end{aligned} \tag{33}$$

Considering the leading-order $\log(y/2Re\sqrt{f})$ term in Eq. (26) gives the Townsend-Perry constant

$$A_1 = \frac{2C\rho^{1/2} y \langle |w_x| \rangle}{\sqrt{\langle \tau_0 \rangle}}, \tag{34}$$

and the generalized Townsend-Perry constants

$$A_p = \frac{2C\rho^{1/2} y \langle |w_x|^p \rangle^{1/p}}{\sqrt{\langle \tau_0 \rangle}}, \tag{35}$$

by use of Eq. (27). This justifies the form of the stress tensor assumed in Ref. [12] and used in Ref. [15]. Finally, we get the expressions

$$A_1 = K\langle |w(x+y) - w(x-y)| \rangle \tag{36}$$

and

$$A_p = K\langle |w(x+y) - w(x-y)|^p \rangle^{1/p}, \tag{37}$$

where K is a constant and this produces the relationship between the Townsend-Perry and the generalized Townsend-Perry constants and the structure function of turbulence; see Refs. [13,14,16] used in Refs. [12,15],

$$A_1 = KC_1 |y^*|^{\zeta_1}, \tag{38}$$

$$A_2 = KC_2^{1/2} |y^*|^{\zeta_2/2}, \tag{39}$$

and

$$A_p = KC_p^{1/p} |y^*|^{\zeta_p/p}, \tag{40}$$

where $-y \leqslant y^* \leqslant y$. Considering the ratio, washes out the constant K,

$$\frac{A_p}{A_2} = \frac{C_p^{1/p}}{C_2^{1/2}} |y^*|^{\zeta_p/p - \zeta_2/2}, \tag{41}$$

where the C_ps and ζ_p are, respectively, the Kolmogorov-Obukhov coefficients and the Kolmogorov-Obukhov scaling exponents, with intermittency corrections of the structure functions from Refs. [13,14,16]. The last ratio was used in Ref. [15] to get agreement between experimental data and theory.

VI. THE SPECTRAL THEORY OF MEAN-SQUARE FLUCTUATIONS

In the above sections we have not used the spectral information in the integral I in Eq. (7). We have just used the attached eddy hypothesis and set $I = 0$ in the viscous layer and $I = 1$ in the inertial layer. But following Ref. [18], we can now use the spectral information through the integral I to find the beginning of the buffer layer and the form of both the MVP U and the fluctuation w in the buffer layer and in the wake. This allows one to obtain the full functional form of both U and w as functions of the distance y from the wall

and compare it with the experimental data in the next section. By use of the energy Eq. (11) and the relation $\eta = \nu^{3/4}\epsilon^{-1/4}$, we can find an expression for η/y, the viscosity parameter that increases as we approach the wall $y \to 0$. If we set the fluctuation equal to zero,

$$\eta/y = (\tilde{u}'(1 - \tilde{y}/Re\sqrt{f}) - (\tilde{u}')^2)^{-1/4}\tilde{y}^{-1} \tag{42}$$

and find a formula for $\tilde{y}$ using this equation along with the equation

$$\kappa^2\tilde{y}^2(u')^2I^{3/4} + u' = \left(1 - \frac{\tilde{y}}{Re\sqrt{f}}\right). \tag{43}$$

The resulting formula is given in Ref. [18],

$$\tilde{y} = \left(\frac{(\eta/y)^{4/3} + \kappa^{4/3}I^{1/2}(\eta/y, 0)}{\kappa^{2/3}(\eta/y)^{8/3}I^{1/4}(\eta/y, 0)}\right). \tag{44}$$

It gives the minimum value of $\tilde{y}$ for which $I(\eta/y, 0) > 0$ and the small eddies begin to contribute to the turbulent shear stress $\tau_t > 0$. In fact, for each value of the parameter β_d, there is a minimum value of $\tilde{y}$ denoted $\tilde{y}_v$ below which $I = 0$. Only after this minimum does $\tilde{y}$ increase with η/y. This gives the end of the viscous layer and the beginning of the buffer layer and a value of the MVP, u_v at $\tilde{y}_v$. It also gives the value of the fluctuation w at $\tilde{y}_v$ and we can integrate the differential equations for u and w, with respect to y, to get the form of both functions in the buffer layer, the inertial layer, and the wake. Along with the formulas in the viscous layer, this gives the full functional form. The differential equations use the spectral information through the full functional form of I and the two parameters β_d and β_e must be fitted to experimental data.

Approximations to the MVP and mean-square fluctuations, based on the formulas in Sec. IV, are given in Figs. 3 and 4, respectively. To compare with experimental data, one must solve the differential equations, from Eq. (16), for only the mean velocity U,

$$U' = -\frac{1}{2\kappa^2I^{3/4}y^2} + \frac{1}{\kappa I^{3/8}y}\sqrt{1 - \frac{y}{Re\sqrt{f}} + \frac{1}{4\kappa^2I^{3/4}y^2}}, \tag{45}$$

with the boundary condition $U = 4.17$ at the beginning of the buffer layer $y = 4.17$. For the fluctuation we first have to solve the differential equation, from Eq. (16), for the fluctuation w after subtracting U and ignoring term of order $O(1/y^3)$ and higher,

$$w' = \frac{\sqrt{\tau_0} - \sqrt{\langle\tau_0\rangle}}{\kappa I^{3/8}y\sqrt{\langle\tau_0\rangle}}\sqrt{1 - \frac{y}{Re\sqrt{f}}}, \tag{46}$$

with the initial condition $w = \frac{\tau_0 - \langle\tau_0\rangle}{\langle\tau_0\rangle}(4.17 - \frac{17.39}{2Re\sqrt{f}})$ at the beginning of the buffer layer.

The parameters β_e and β_d are fixed by the fit of the mean velocity U to the experimental data; see Ref. [18]. Unlike the mean velocity, the best fit of w with the viscous profile $w = \frac{\tau_0 - \langle\tau_0\rangle}{\langle\tau_0\rangle}(y - \frac{y^2}{2Re\sqrt{f}})$ is not always at $y_0 = 4.17$, so we let the initial condition y_0 vary to get a best fit with the viscous profiles in Fig. 4.

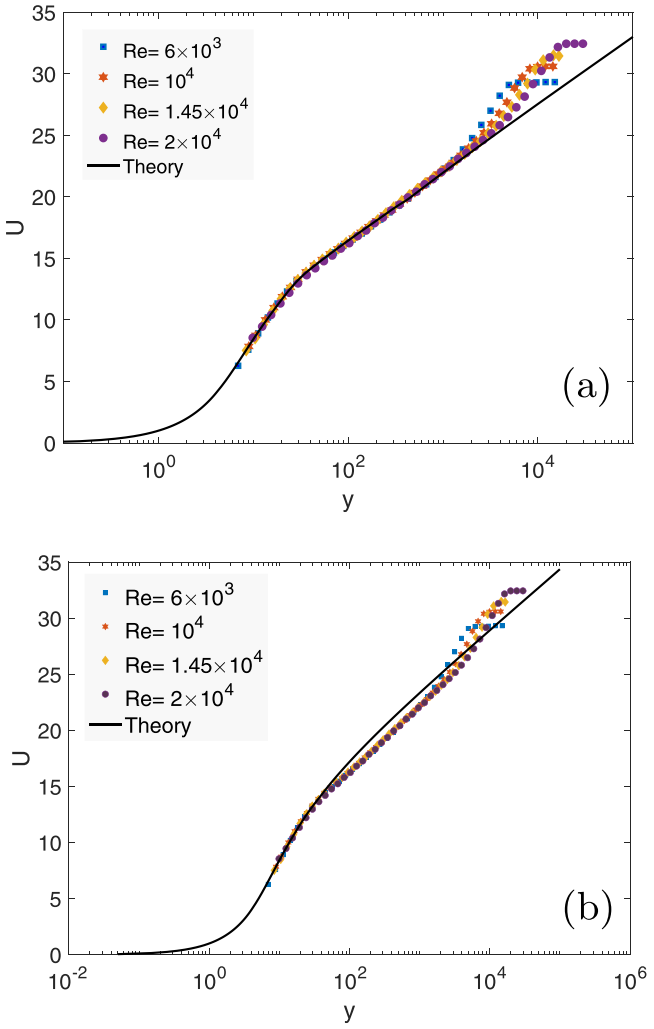

FIG. 3. The average of the MVP as a function of $log(y)$, where y is the distance from the wall. Experimental data are plotted in the dotted curves corresponding to different Re numbers, and the theoretical prediction is given in the black curve. (a) The theoretical curve is determined by a spectral I function $\alpha I(y) + (1 - \alpha)I_b(y)$ that interpolates between the $k^{-5/3}$ and the k^{-1} with $\alpha \leqslant 1$ in the buffer region. (b) The theoretical curve has only the $I(y)$-integral with the $k^{-5/3}$ scaling present in buffer and inertial regions.

VII. COMPARISON WITH EXPERIMENTAL DATA

The data we use to compare with the theory come from the wind tunnel experiments at the University of Melbourne using the nano-scale thermal anemometry probe (NSTAP) to conduct velocity measurements in the high Re number boundary layer up to $Re_\tau = 20000$. The NSTAP has a sensing length almost one order of magnitude smaller than conventional hot wire; hence it allows for a fully resolved NSTAP measurement of velocity fluctuations [20,24]. The size of the University of Melbourne wind tunnel and the accuracy of the NSTAP permit the measurement over a very large range of scales. We use the averaged velocity time series at Reynolds numbers $Re_\tau = 6000, 10000, 14500, 20000$ and the averaged variance at the same Reynolds numbers. Figure 3 shows the mean velocity profiles as a function of normalized distance from the wall, whereas Fig. 4 shows the averaged fluctuation squared

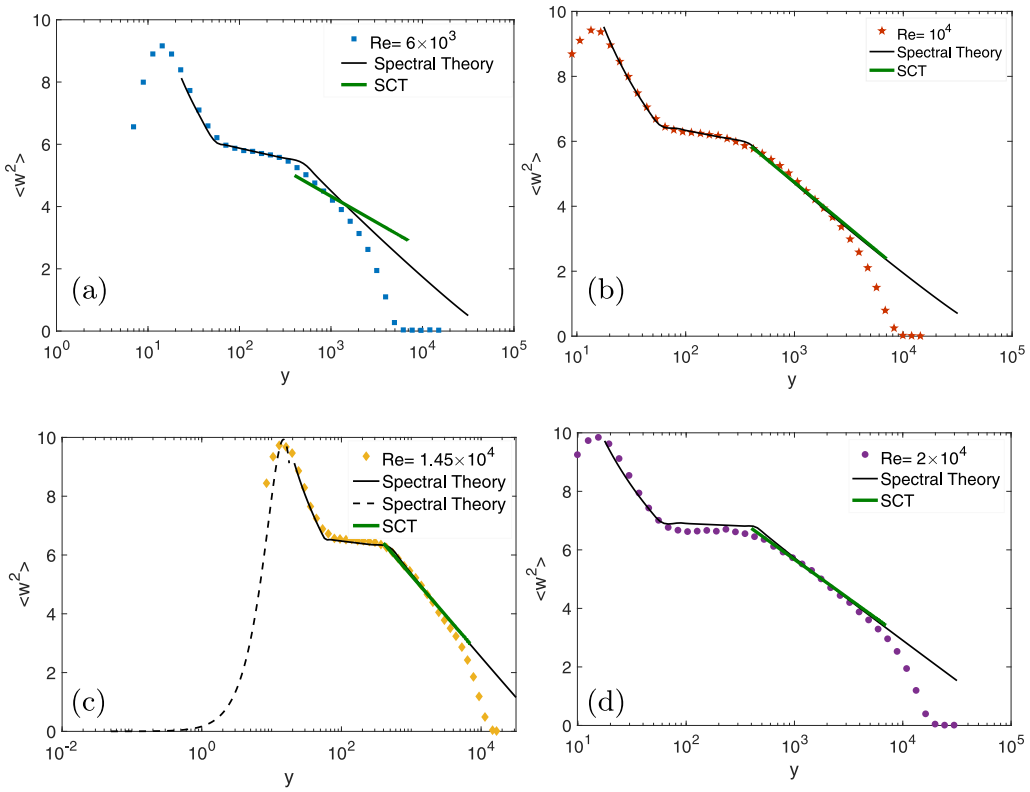

FIG. 4. The average of the fluctuation squared as a function of $log(y)$, where y is the distance from the wall (dimensionless units). Comparison of experimental data (dotted curves for different Re numbers) with the theoretical curves give. The theoretical curve is determined by a spectrum I function $\alpha I(y) + (1-\alpha)I_b(y)$ that interpolates between the $k^{-5/3}$ to the k^{-1} with $\alpha \ll 1$ in the buffer region. The straight lines correspond to the log law with the Towsend-Perry constants predicted by the SCT.

(variation) as a function of the normalized distance to the wall. Both are semilog plots.

First, let us consider the curve describing the MVP in Fig. 3(b). It starts with the viscous profile because the I function is zero. But then we reach the value y_v where the first attached eddies appear ($y = 4.17$) and then the viscous profile changes; instead of reaching its maximum $u = Re\sqrt{f}/2$ at $y = Re\sqrt{f}$, the attached eddies increase the viscosity (decrease the Re number) and the MVP reaches its maximum increase at $y \approx 15$, independent of the Reynolds number. The energy transfer of the attached eddies is captured by the I integral and we integrate the differential equation given by Eq. (45), from $y = 4.17$, with the initial condition $u = 4.17$. This gives the MVP in Fig. 3(b). This was already done in Ref. [18] and describes how the attached eddies transfer energy into the buffer and the inertial layer. However, we notice that in the predicted MVP overestimates the mean velocity in buffer region. This is because the I function from Eq. (7) does not account for the formation of the detached eddies, which reduce the net energy transfer in the direct cascade.

The curves for the fluctuations squared in Fig. 4 are obtained in a similar manner. The attached eddies fix the peak of $\langle w^2\rangle$ at $y \approx 15$ and the peak profiles can be fitted by the viscous formula $\langle w^2\rangle = a(y - \frac{y^2}{30})^2$ where $a \sim (\langle \tau_o^2\rangle - \langle \tau_o\rangle^2)/\langle \tau_o\rangle^2$. This fit is shown in Fig. 4(c). The peak position is experimentally observed to be fixed, but its height shows a weak Reynolds number dependence $a = -3.06 + 0.99\log(Re)$; see Ref. [20]. This relationship can be tested using our theory; see also Ref. [25] for more discussion. Then, we integrate the differential equation from Eq. (46) for w with the initial data described in the last section from some point to the right of the peak, where the above peak profile fits the initial condition; this gives the profile of the fluctuations squared, down to the flat part in the buffer layer. At the beginning of the flat part, $y \approx 60$, the second scaling from Sec. II begins to dominate the fluctuations, modeling the $1/k$ scaling of detached eddies in the buffer layer. Then we use interpolate between the two spectral functions, such that $I_b(y)$ dominates for values of y in the buffer region, and $I(y)$ takes over for values of y in the inertial region where the Kolmogorov-Obukhov scaling dominates again and the attached eddies break up. This produces the curves in Fig. 4.

We can now compare the mean-square fluctuations shown in Fig. 4 with the predictions of the SCT of turbulence, used in Refs. [12,15], to compute the Townsend-Perry constants in the inertial (log) layer. These computations use the first structure function S_1 of turbulence and we explain how they are performed; see Refs. [12,15] for more information. The computed Townsend-Perry constants are listed in Table I.

The first structure function of turbulence is (see Ref. [16])

$$E(|u(x,t) - u(y,t)|) = S_1(x,y,t)$$
$$= \frac{2}{C}\sum_{k\in\mathbb{Z}^3\setminus\{0\}} \frac{|d_k|(1-e^{-\lambda_k t})}{|k|^{\zeta_1} + \frac{4\pi^2\nu}{C}|k|^{\zeta_1+\frac{4}{3}}} |\sin(\pi k\cdot(x-y))|,$$

TABLE I. Here the approximate A_1 value is computed from C_1 using the proportionality factor $A_1 = C_1/(K|y^*|^{\zeta_1}) = C_1/12.952$.

Re_λ	C_1	A_1	B_1
6000	9.449	0.730	9.373
10,000	15.628	1.207	13.073
14,500	15.500	1.197	13.573
20,000	14.994	1.158	13.673

where the Re number dependence enters through the viscosity ν, and E denotes the expectation (ensemble average). To get the Kolmogorov-Obukhov coefficients, C_p in

$$S_p(r,\infty) \sim C_p r^{\zeta_p}, \tag{47}$$

for the lag variable r small, and ζ_p the scaling exponents, we send t to ∞ in the above formulas and project onto the longitudinal lag variable $\mathbf{r} = (r, 0, 0)$. For $p = 1$, this becomes

$$S_1 \sim \frac{2\pi^{\zeta_1}}{C} \sum_{k\neq 0} \frac{|d_k|}{(1+\frac{4\pi^2\nu}{C}|k|^{4/3})} r^{\zeta_1}$$

$$= \frac{4\pi^{\zeta_1}}{C} \sum_{k=1}^{\infty} \frac{a}{(a^2+k^m)(1+\frac{4\pi^2\nu}{C}|k|^{4/3})} r^{\zeta_1}, \tag{48}$$

see Ref. [16]; where $\zeta_1 = 0.37$, see Ref. [13]. Now we use the values for ν in Table 1 in Ref. [15] and the corresponding values for a, m, and C from Table 3 in the same paper. The Re numbers, 6430, 10,770, 15,740, and 19,670 are close enough to the experimental ones such that we can use the value of the parameters in Ref. [15]. This gives the values in Table I, where $A_1 \sim K|y^*|^{\zeta_1}C_1$, see Sec. V, and the proportionality factor $K|y^*|^{\zeta_1} = 1/12.952$ is computed at the Re number 15,470, where the approximated A_1 coincides with the measured A_1. The log functions with coefficient A_1, from the third column in Table I, and using the constant B_1 from the fourth column in Table I, are then compared to the experimental and theoretical values in Fig. 4. The spanwise Townsend-Perry constants, for the spanwise fluctuations, can computed similarly by projecting onto the spanwise lag variable $\mathbf{t} = (0, t, 0)$.

In Fig. 4(a), the Townsend-Perry constant A_1 computed by the SCT does not agree with the measured slope. This was already observed in Ref. [15], since for low Reynolds numbers the C_1s do not provide a good approximation to the A_1s. They only do for large Reynolds numbers and the discrepancy (a) occurs at the smallest Reynolds number. This does not happen for the Generalized Townsend-Perry constants, the reasons are explained in Ref. [15], and for them the C_ps, $p \geqslant 2$ provide good approximations to the A_ps for all Reynolds numbers.

VIII. DISCUSSION

We used the spectral theory of the MVP and the variation profile to represent both and compare with experiment [20] for a range of Reynolds numbers. Assuming that the wall shear stress is a fluctuating quantity, we can derive the log law for the variation (2) that was proposed by Townsend and measured by Perry and Chong. This law involves the Townsend-Perry constants. This was first done in the large Reynolds number limit and then for general Reynolds numbers. The Reynolds number dependence of the Townsend-Perry constants is determined by the SCT [12,15]. We derive the log law for the higher moments of the fluctuations and the generalized Townsend-Perry constants based on the functional form of the variation and use the SCT to express them in terms of the Kolmogorov-Obukhov coefficients of the structure functions of turbulence [16]. This confirms the results in Refs. [12,15].

The spectral function I derived in Ref. [18] plays a central role in this theory. It can be considered to be the analytic expression of Townsend's theory of wall-attached eddies. It quantifies when the first eddies appear at the boundary of the viscous and the buffer layer and when they are fully developed in the inertial layer. It even quantifies the limit of their influence in the energetic wake. By introducing the spectral theory into the analysis, it resolves many of the issues that we are faced with in boundary layer turbulence.

The I function corresponds to the Kolmogorov-Obukhov cascade $k^{-5/3}$ in the inertial layer, but in the buffer layer another cascade k^{-1} dominates the fluctuations, although its influence on the MVP is small. This is a scaling at constant energy, $1/k$ in Fourier space, that shrinks (the cross-section of) and accelerates detached eddies. The energy transfer of this cascade is captured by the I function in buffer layer, I_b. With it we are able to produce the functional form of the averaged fluctuations square in the buffer layer. Once in the inertial layer the original I function dominates again.

The final confirmation of this spectral theory is how we are able to improve the fit to experimental values of the MVP in Ref. [18] by use of the I_b function in the buffer layer. Although this effect on the MVP is small, the detached eddies siphon a small amount of energy from the MVP in the buffer layer. We model this by linear combination of the I and I_b function $(1-\alpha)I + \alpha I_b$, in the buffer layer, where a is small. This produces a better fit to the measured MVP in the buffer region as shown in Fig. 3(a), whereas the fit without this linear combination, shown in Fig. 3(b), is not as good.

A formulation of the unstable vortices and streaks found by Kline *et al.* [26] and the formulation of structures forming in the wake are still missing from our theory. However, with these results as a basis, hopefully such structures can also be added.

It is fair to ask what the Townsend attached eddies actually look like since our spectral method is based on them. Unlike the streamwise streaks and associated vortices that have been visualized since the experiments of Kline *et al.* in the 1960s (see Refs. [26,27]), the attached eddies are difficult to visualize either in experiments or in simulations. We provide a sketch in Fig. 5, where streamwise streaks are visualized gradually lifting from the boundary by the flow, and perpendicular to them are spanwise attached eddies being deformed by the alternating slow and fast streamwise flow into a hairpin vortex. This does happen both in experiments and in observations; see Ref. [28]. However, these hairpin vortices are made unstable by the striations in the streamwise flow, and the typical attached eddies are irregular in shape with the general feature of being stretched by the flow and attached to the wall. In general, the hairpin vortices break up into

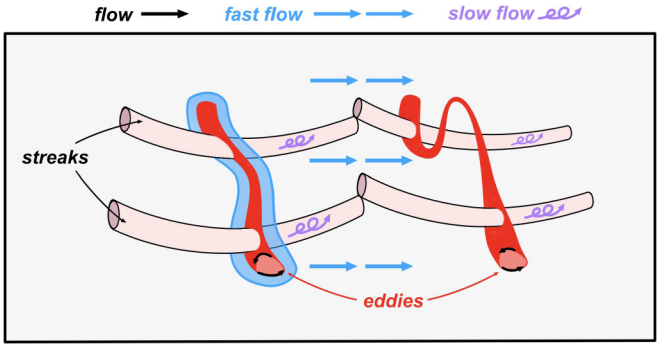

FIG. 5. Sketch of the instantaneous streaks, in the streamwise direction, and the wall-attached eddies in the spanwise direction.

wall-attached eddies in the streaks and wall-detached eddies on the buffer layer side of the (Kline) streamwise vortices. One must interpret their influence in a statistical sense.

ACKNOWLEDGMENTS

We are thankful to Ivan Marusic, Milad Samie, and Christian E. Willert for kindly sharing with us the wind turbulence experimental data and Joe Klewicki for useful conversations. We are grateful to Knut Bauer for proving us with the graphic illustrations. This research was supported in part by the National Science Foundation Grant No. NSF PHY-1748958 through the Kavli Institute for Theoretical Physics.

[1] J. C. Wyngaard, Atmospheric turbulence, Annu. Rev. Fluid Mech. **24**, 205 (1992).
[2] F. Toschi and E. Bodenschatz, Lagrangian properties of particles in turbulence, Annu. Rev. Fluid Mech. **41**, 375 (2009).
[3] W. Vinen and J. Niemela, Quantum turbulence, J. Low Temp. Phys. **128**, 167 (2002).
[4] A. J. Smits and I. Marusic, Wall-bounded turbulence, Phys. Today **66**(9), 25 (2013).
[5] J. Jiménez, Near-wall turbulence, Phys. Fluids **25**, 101302 (2013).
[6] M. Oberlack, *Self-Similar Mean Velocity Profiles in Plane Parallel Turbulent Shear Flows* (Delft University Press, Delft, 1997).
[7] X. Chen, F. Hussain, and Z.-S. She, Non-universal scaling transition of momentum cascade in wall turbulence, J. Fluid Mech. **871**, R2 (2019).
[8] L. Prandtl, *Essentials of Fluid Dynamics: With Applications to Hydraulics, Aeronautics, Meteorology and Other Subjects* (Hafner Publishing Company, New York, 1952).
[9] A. E. Perry and M. S. Chong, On the mechanism of wall turbulence, J. Fluid Mech. **119**, 173 (1982).
[10] A. Perry, S. Henbest, and M. S. Chong, A theoretical and experimental study of wall turbulence, J. Fluid Mech. **165**, 163 (1986).
[11] C. Meneveau and I. Marusic, Generalized logarithmic law for high-order moments in turbulent boundary layers, J. Fluid Mech. **719**, R1 (2013).
[12] B. Birnir and X. Chen, Sub-Gaussian behavior of the Townsend-Perry constants in turbulent boundary layers, Phys. Rev. E **93**, 011101 (2016).
[13] B. Birnir, The Kolmogorov-Obukhov statistical theory of turbulence, J. Nonlinear Sci. **23**, 657 (2013).
[14] B. Birnir, *The Kolmogorov-Obukhov Theory of Turbulence* (Springer, New York, 2013).
[15] J. Kaminsky, B. Birnir, and J. Klewicki, The application of the stochastic closure theory to the generalized Townsend-Perry constants, Phys. Rev. E **100**, 061101 (2019).
[16] J. Kaminsky, B. Birnir, G. Bewley, and M. Sinhuber, Reynolds number dependence of the structure functions in homogeneous turbulence, J. Nonlinear Sci. **30**, 1081 (2020).
[17] A. A. Townsend, *The Structure of Turbulent Shear Flow* (Cambridge University Press, Cambridge, UK, 1976).
[18] G. Gioia, N. Guttenberg, N. Goldenfeld, and P. Chakraborty, Spectral Theory of the Turbulent Mean-Velocity Profile, Phys. Rev. Lett. **105**, 184501 (2010).
[19] M. Lee and R. Moser, DNS of turbulent channel flow up to $\mathrm{Re}_\tau \approx 5200$, J. Fluid Mech **774**, 395 (2015).
[20] M. Samie, I. Marusic, N. Hutchins, M. Fu, Y. Fan, M. Hultmark, and A. Smits, Fully resolved measurements of turbulent boundary layer flows up to $Re_\tau = 20000$, J. Fluid Mech. **851**, 391 (2018).
[21] J. Vassilicos, J.-P. Laval, J.-M. Foucaut, and M. Stanislas, The streamwise turbulence intensity in the intermediate layer of turbulent pipe flow, J. Fluid Mech. **774**, 324 (2015).
[22] F. Toschi, G. Amati, S. Succi, R. Benzi, and R. Piva, Intermittency and Structure Functions in Channel Flow Turbulence, Phys. Rev. Lett. **82**, 5044 (1999).
[23] Y. Hwang and Y. Bengana, Self-sustaining process of minimal attached eddies in turbulent channel flow, J. Fluid Mech. **795**, 708 (2016).
[24] R. Baidya, W. Baars, S. Zimmerman, M. Samie, R. J. Hearst, E. Dogan, L. Mascotelli, X. Zheng, G. Bellani, A. Talamelli *et al.*, Simultaneous skin friction and velocity measurements in high Reynolds number pipe and boundary layer flows, J. Fluid Mech. **871**, 377 (2019).
[25] X. Chen and K. R. Sreenivasan, Reynolds number scaling of the peak turbulence intensity in wall flows, J. Fluid Mech. **908**, R3 (2021).
[26] S. J. Kline, W. C. Reynolds, F. Schraub, and P. Runstadler, The structure of turbulent boundary layers, J. Fluid Mech. **30**, 741 (1967).
[27] J. Jiménez and A. Pinelli, The autonomous cycle of near-wall turbulence, J. Fluid Mech. **389**, 335 (1999).
[28] I. Marusic and J. P. Monty, Attached eddy model of wall turbulence, Annu. Rev. Fluid Mech. **51**, 49 (2019).